ACS Catalysis

Letter

Cite This: ACS Catal. 2018, 8, 4996−5001

pubs.acs.org/acscatalysis

Influence of Atomic-Level Morphology on Catalysis: The Case of Sphere and Rod-Like Gold Nanoclusters for CO_2 Electroreduction

Shuo Zhao,[†] Natalie Austin,[‡] Mo Li,[†] Yongbo Song,[†] Stephen D. House,[§] Stefan Bernhard,[†] Judith C. Yang,[§] Giannis Mpourmpakis,*[,‡] and Rongchao Jin*[,†]

[†]Department of Chemistry, Carnegie Mellon University, Pittsburgh, Pennsylvania 15213, United States

[‡]Department of Chemical Engineering, University of Pittsburgh, Pittsburgh, Pennsylvania 15261, United States

[§]Chemical and Petroleum Engineering, and Physics, University of Pittsburgh, Pittsburgh, Pennsylvania 15261, United States

Supporting Information

ABSTRACT: Gold-based materials hold promise in electrocatalytic reduction of CO_2 to fuels. However, the polydispersity of conventional gold nanostructures limits mechanistic studies. Here, we report two types of atomically precise Au_{25} nanoclusters (1 nm) with distinct morphology (i.e., nanosphere and nanorod) for CO_2 reduction catalysis. The Au_{25} nanosphere exhibits higher Faradaic efficiency for CO with higher formation rates compared to the Au_{25} nanorod. First-principles calculations reveal that the negative charge and the energetically favorable removal of one ligand to generate an active site on the nanosphere can better stabilize the important *COOH intermediate in CO_2 electroreduction.

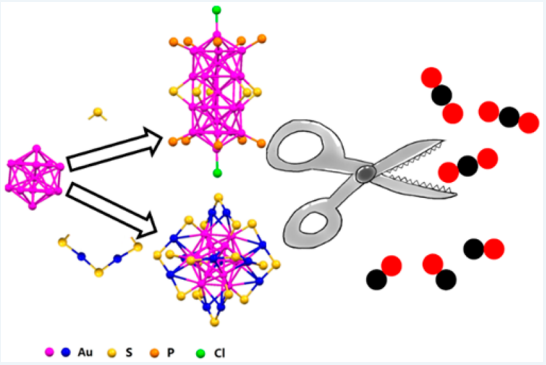

KEYWORDS: *gold nanoclusters, atomic precision, morphology, CO_2 electroreduction*

Ultrasmall, ligand-protected metal nanoclusters constitute an emerging class of novel nanomaterials and possess precise compositions and structures as well as extremely large surface-to-volume ratios, which are promising for heterogeneous catalysis.[1−4] Atomically precise, thiolate-protected gold nanoclusters (denoted as $Au_n(SR)_m$, where n and m are the numbers of gold atoms and thiolate ligands, respectively) have received intense interest owing to their high stability and molecular purity, as well as the availability of structures solved by X-ray crystallography.[5,6] In terms of the electronic properties, gold nanoclusters consisting of a few tens to several hundred atoms (1−3 nm) constitute the size regime from molecular-like (e.g., with a sizable HOMO−LUMO gap) to plasmonic nanoparticles (e.g., metallic state).[5] The special size regime and strong quantum confinement of electrons impart metal nanoclusters with unique properties and thus such nanoclusters hold great promise in diverse applications such as catalysis,[7−14] sensing,[15,16] optics,[17−20] and energy-conversion processes.[21,22]

With respect to research on CO_2 conversion, it is well-known that the heavy reliance on fossil fuels leads to the release of excessive amounts of CO_2 and causes global warming issues. Thus, converting greenhouse gas to energy-dense fuels by electrochemistry techniques is a promising way to mitigate atmospheric CO_2.[23,24] Gold-based catalysts such as Au nanoparticles and nanowires show excellent activity as well as high selectivity toward CO.[25−32] Gold nanoparticles were reported to exhibit size-dependent catalytic activity and selectivity.[26] Morphology control and surface engineering of the catalysts have been recognized as effective ways for tuning the catalytic performance.[27−30] However, fundamental understanding of CO_2 catalytic reduction is still limited by the polydispersity and ill-defined surfaces of conventional nanocatalysts. For example, quite different catalytic performance could be observed from nanoparticles of identical size, because such nanocatalysts, though being the same size (e.g., 5 nm), may have quite different surface structures and atomic-level morphology.[26] In this context, atomically precise gold nanoclusters with uniform structure are particularly attractive and hold great promise in fundamental studies.[33−36] Kaufmann et al. first reported the utilization of gold nanoclusters for CO_2 electroreduction to CO with high selectivity.[33] Compared to conventional nanocatalysts, atomically precise gold nanoclusters can serve as a well-defined platform for mechanistic studies.[36]

In this work, we investigate two types of Au nanoclusters of identical size (i.e., 25 atoms) but distinctly different atomic packing structures or morphology (i.e., Au_{25} nanosphere and Au_{25} nanorod) as electrocatalysts for CO_2 reduction. Interestingly, the Au_{25} sphere exhibits constantly higher activity and selectivity for CO_2 reduction to CO than the Au_{25} rod does. Based on density functional theory (DFT) calculations,

Received: January 27, 2018
Revised: April 12, 2018
Published: April 26, 2018

DOI: 10.1021/acscatal.8b00365
ACS Catal. 2018, 8, 4996−5001

we attribute the higher catalytic performance of the Au_{25} nanosphere to its negative charge and the energetically favorable exposure of an active site on the nanosphere that stabilizes the key *COOH intermediate.

The syntheses of Au_{25} nanosphere and nanorod clusters followed the reported protocols.[37,38] The UV−vis spectra are characteristic of specific nanoclusters (different sizes or shapes) and thus can conveniently be used to confirm the purity. As shown in Figure 1a,b, the Au_{25} nanosphere exhibits distinct

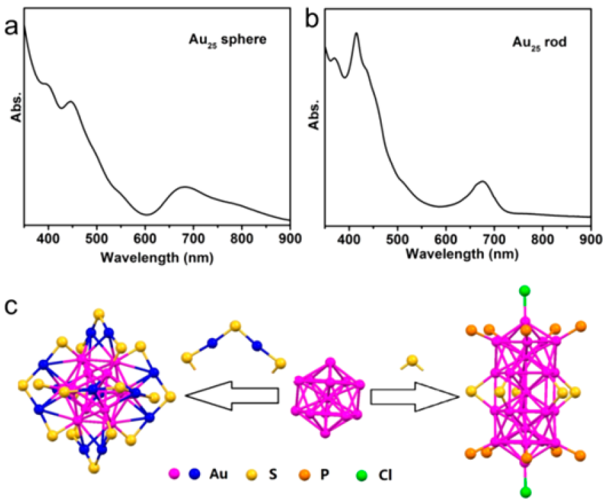

Figure 1. UV−vis spectra of Au_{25} nanosphere (a) and nanorod (b). (c) Atom packing structures of Au_{25} nanosphere and nanorod.

peaks at 400, 445, and 685 nm while Au_{25} nanorod shows absorption bands at 415 and 670 nm. These absorption features are spectroscopic fingerprints for the Au_{25} nanosphere and nanorod clusters and thus indicate their purity. Figure 1c shows the atom packing structures of the Au_{25} nanosphere and nanorod solved by X-ray crystallography.[39,40] The Au_{25} nanosphere comprises an icosahedral Au_{13} core protected by six dimeric surface staples (-SR-Au-SR-Au-SR-), giving rise to a quasi-spherical core−shell morphology. In the Au_{25} nanorod, two Au_{13} icosahedra share one vertex gold atom and are joined together by five bridging thiolates (-SR-) at the rod's waist. The remaining 10 phosphine ligands and 2 chlorides are evenly distributed to the two ends of the nanorod. The different atomic-level morphologies of these two nanoclusters may potentially affect their CO_2 electrocatalytic reduction performance.

Scanning transmission electron microscopy (STEM)[49] was further employed to image the Au_{25} nanosphere and nanorod clusters. Figure 2a,b show typical STEM images of as-synthesized Au_{25} nanosphere and nanorod clusters. Their size (~1 nm) and monodispersity are confirmed by statistical analysis of size in Figure 2c,d, respectively (see the Supporting Information for more details). Notably, because the STEM is not aberration-corrected, it is unable to resolve the atomic-level structural morphology difference between the Au_{25} nanosphere and nanorod clusters. Figure 2e,f display the Au_{25} nanosphere and nanorod clusters loaded on carbon black support (as catalysts for CO_2 reduction, vide infra), which show well-dispersed Au_{25} nanoclusters on the surface of the carbon black support. The statistical size distribution analysis in Figure S2 provides strong evidence that all ligands still remain on the nanoclusters when supported on carbon black support.

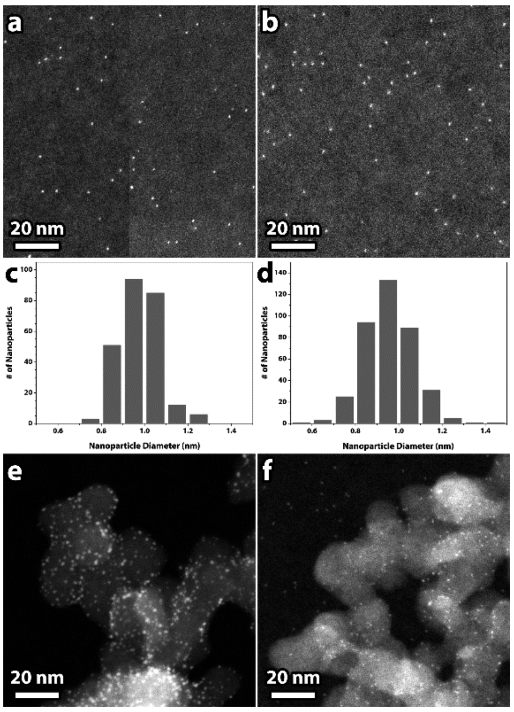

Figure 2. STEM images and particle size histograms of Au_{25} nanosphere (a,c) and nanorod (b,d). STEM images of Au_{25} nanosphere (e) and nanorod (f) supported on carbon black.

The gold nanoclusters (supported on carbon black support, Vulcan XC-72R, with 10 wt % loading) were then evaluated for the electrocatalytic CO_2 reduction. Figure 3 compares the CO_2

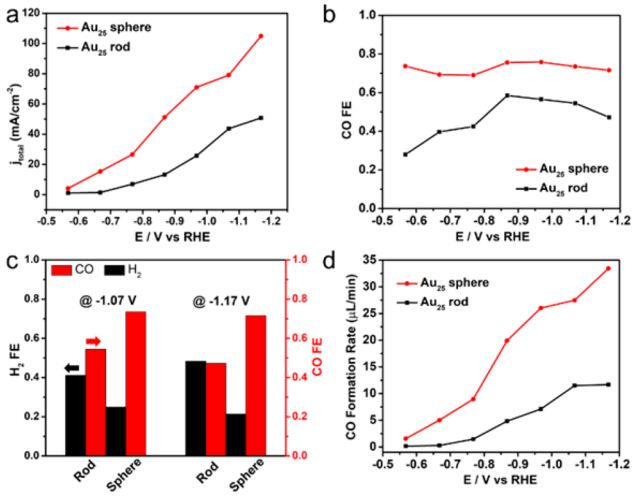

Figure 3. Electrocatalytic CO_2 reduction performance of the two Au_{25} nanoclusters. (a) Total current density of CO_2 reduction, (b) Faradaic Efficiency (FE) for CO production over Au_{25} nanosphere and nanorod catalysts, (c) FEs for CO and H_2 at the potential of −1.07 and −1.17 V over Au_{25} nanosphere and nanorod, respectively. (d) CO formation rates over Au_{25} nanosphere and nanorod.

reduction performance of Au_{25} nanosphere and nanorod clusters. As shown in Figure 3a, the total current density values for the Au_{25} nanosphere cluster at all potentials are larger than the corresponding values of the Au_{25} nanorod cluster, indicating higher catalytic performance of the Au_{25} nanosphere. The selectivity of the catalysts in CO_2 reduction is crucial in

DOI: 10.1021/acscatal.8b00365
ACS Catal. 2018, 8, 4996−5001

practical applications due to the competing water reduction generating H_2 as well as the formation of CO_2 reduction products other than CO. As for the distribution of carbon-containing products, gold nanoclusters exhibit excellent selectivity for the CO product[33] than other carbon-containing products. Only CO and H_2 were detected in all our experiments, which is consistent with previous results.[33−35] Figure 3b compares the FE for CO over the Au_{25} nanosphere and nanorod clusters. The Au_{25} nanosphere cluster shows higher FE toward CO than the Au_{25} nanorod cluster under all voltages. The better catalytic performance of the Au_{25} nanosphere is more distinct under high voltages where the Au_{25} nanosphere cluster exhibits a FE of 73.7% at −0.57 V, which is 1.63 times higher than that of the Au_{25} nanorod cluster (FE ∼ 28.0%). At −0.67 V, a FE difference of 30% (i.e., 69.3% vs 39.7%) between the two clusters is also prominent in Figure 3b. Figure 3c shows the selectivity of the two Au_{25} nanoclusters in electrocatalytic CO_2 reduction at the potential of −1.07 V and −1.17 V, respectively. At −1.07 V, the FE for CO (73.5%) is much higher than that for H_2 (24.9%), which indicates that the competing water reduction reaction is significantly suppressed by the reduction of CO_2 to CO. While the Au_{25} nanorod also produces more CO than H_2, the Au_{25} nanosphere exhibits much higher selectivity with smaller FE toward H_2 compared to the Au_{25} nanorod. At −1.07 V, the Au_{25} nanosphere shows FE of 24.9% toward H_2, which is much lower than that of Au_{25} nanorod (41.2%).

Besides the high FE for CO, the Au_{25} nanosphere also produces CO at higher rates than the nanorod. Figure 3d compares the CO formation rates over the two Au_{25} catalysts under all voltages, where the Au_{25} nanosphere shows much higher CO formation rates than the Au_{25} nanorod does. The difference in the CO formation rate between the two clusters becomes more significant as the voltage moves negatively (i.e., at more reducing power). At −1.17 V, the CO formation rate of the Au_{25} nanosphere reaches 33.3 μL/min, which is 2.8 times that of Au_{25} nanorod (11.7 μL/min). The larger FE for CO as well as higher CO formation rates over Au_{25} nanosphere consistently demonstrate its higher catalytic performance for CO_2 reduction compared to the Au_{25} nanorod.

Our experiments clearly show the Au_{25} nanosphere possesses higher CO_2 reduction activity and selectivity for CO product than the Au_{25} nanorod. To further understand their different catalytic behavior, DFT calculations were performed[41−48] (see the Supporting Information for details). In recent work, Alfonso et al. assessed CO_2 reduction to CO on the fully protected $Au_{25}(SCH_3)_{18}^-$ spherical nanocluster as well as the partially ligand-removed $Au_{25}(SCH_3)_{17}^-$ spherical nanocluster.[36] They determined that the $Au_{25}(SCH_3)_{17}^-$ species would promote CO_2 reduction more favorably, compared to the $Au_{25}(SCH_3)_{18}^-$, because the $Au_{25}(SCH_3)_{17}^-$ species stabilized the *COOH intermediate on the exposed Au atoms of the ligand-removed site. Therefore, the removal of one ligand from the nanoclusters is critical for generating active sites for CO_2 reduction. As a result, herein we first compare the ability of the two nanoclusters to partially release ligands and expose Au active sites, from the different sites of the nanosphere and nanorod.

Figure 4a illustrates the two nanoclusters and sites from which ligands are removed. For the nanosphere, removal of a single -SCH_3 is considered, whereas for the nanorod, removal of -SCH_3, -Cl, or PH_3 is considered. The -SCH_3 and -Cl ligands are removed as reduction reaction steps using hydrogen while

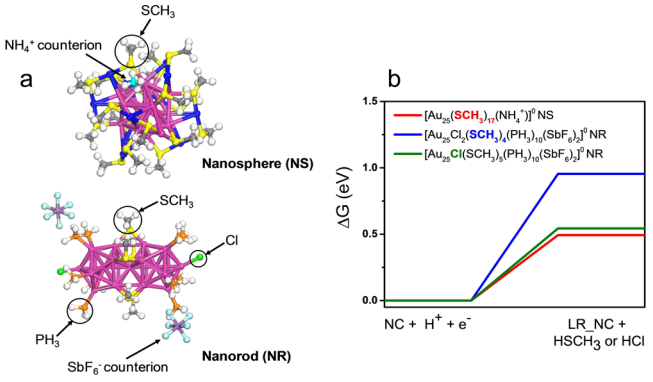

Figure 4. (a) Structures for the nanorod and the nanosphere in the presence of the NH_4^+ and SbF_6^- counterions, respectively. The color code is as shown in Figure 1(c) with the addition of N atoms shown in bright blue, Sb shown in purple, and F shown in light blue. The circled regions on the nanoclusters demonstrate sites of ligand removal on the nanosphere (-SCH_3) and nanorod (-SCH_3, -Cl, and PH_3) (b) ΔG values for ligand removal (in eV) from the nanoclusters at 0 V vs RHE, where LR_NC represents "ligand-removed nanocluster", NS is nanosphere, and NR is nanorod. The blue and green lines represent removing a -SCH_3 and -Cl from the nanorod with SbF_6^- counterions, respectively and the red line represents removing -SCH_3 from the nanosphere with a NH_4^+ counterion. All ligand removal steps are treated as electrochemical reduction steps.

the removal of PH_3 is considered as a desorption step (see Computational methods in Supporting Information). Figure 4b shows the ΔG values for removing different ligands from the nanosphere and nanorod at 0 V vs reversible hydrogen electrode (RHE). Of note, the removal of the PH_3 is not included in Figure 4b due to different pathways (reduction versus desorption steps). The desorption of PH_3 from the nanorod is calculated to be ΔG: 0.54 eV which is equivalent to the removal of -Cl (green line, ΔG: 0.54 eV) as shown in Figure 4b. For the nanorod, the removal of PH_3 and -Cl is more favorable than the removal of -SCH_3 (blue line, ΔG: 0.95 eV). Comparing ligand removal from the nanorod to the nanosphere, the removal of -SCH_3 is less endergonic from the nanosphere (red line, ΔG: 0.49 eV) than from the nanorod. It is observed that ligand removal from the nanosphere is slightly more favored than the ligand removal from the nanorod. Therefore, the ligand removal to release active sites on the nanosphere cluster is more energetically favorable than the nanorod cluster.

After the ligand removal, gold active sites on the nanosphere and nanorod are revealed for CO_2 reduction catalysis. We then calculated the energetics for CO_2 reduction to CO at 0 V vs RHE on the ligand-removed (i.e., active sites) of the nanoclusters. The formation of *COOH (ΔG_{*COOH}) has been shown to be an important intermediate in CO_2 reduction to CO on Au.[26,34] Figure 5 illustrates that *COOH is more stabilized on the $Au_{25}(SCH_3)_{17}NH_4$ (-SCH_3 removed) nanosphere (0.43 eV) than on any of the ligand-removed systems of the nanorod (ΔG_{*COOH}, -SCH_3 removed: 0.65 eV, -Cl removed: 0.56 eV, and PH_3 removed: 1.15 eV). Illustrations of the adsorbed *COOH structures are provided in Figure S3 (see the Supporting Information). It should be noted that even though PH_3 and -Cl can be removed from the nanorod at a comparative ΔG to -SCH_3 removal from the nanosphere, the resulted active species do not stabilize *COOH comparatively as shown in Figure 5. Therefore, the energetically favorable

DOI: 10.1021/acscatal.8b00365
ACS Catal. 2018, 8, 4996−5001

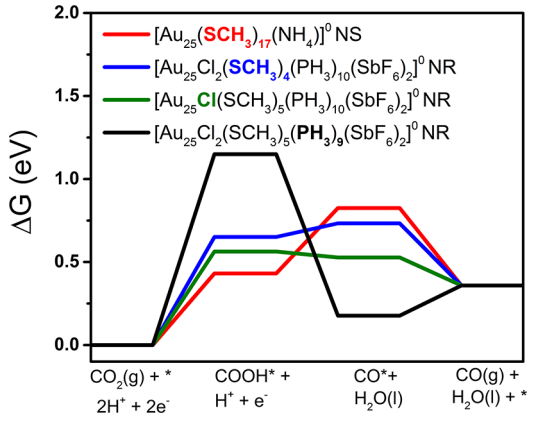

Figure 5. Free energy diagrams (ΔG) for CO_2 reduction to CO on the ligand-removed nanoclusters at 0 V vs RHE. The black, blue, green, and red lines represent CO_2 reduction to CO on the nanorod with PH_3 removed, the nanorod with -SCH_3 removed, the nanorod with -Cl removed, and on the nanosphere with -SCH_3 removed, respectively.

removal of -SCH_3 from the nanosphere to release active sites as well as the stabilization of *COOH over the obtained $Au_{25}(SCH_3)_{17}$ species contribute to the higher catalytic performance of the Au_{25} nanosphere over the Au_{25} nanorod.

Kauffman et al. previously investigated CO_2 reduction on the $[Au_{25}(SCH_3)_{18}]^q$ nanosphere in three charge states (q = +1,0,-1).[34] The negatively charged Au nanocluster was found to promote CO_2 reduction more significantly, compared to the neutral and positively charged nanoclusters, by stabilizing the reaction intermediates. To verify the role of nanocluster's charge on CO_2 reduction, we performed Bader charge analysis calculations and determined that, in the presence of counterions, the nanosphere remained negatively charged (q = −0.77), whereas the nanorod positively charged (q = +1.94). Thus, the negative charge that the nanosphere possesses contributes to its higher activity in CO_2 reduction observed in experiments compared to the nanorod. Thus, overall, the negative charge and the favorable exposure of an active site on the nanosphere stabilize the important *COOH intermediate, which, in turn, contribute to enhanced activity of the nanosphere than the nanorod. Although we have not investigated multiple ligand removal steps from the surface of the nanoclusters, in the Supporting Information we report a preliminary analysis on removing 1 and 2 additional ligands from the nanoclusters (see Figure S5) and find that additional ligand removal remains endothermic, but still probable under the experimentally applied potentials. A thorough analysis of the energetics for multiple ligand removal steps is a future research direction.

In summary, we have investigated the atomic-level morphology effect of Au_{25} nanoclusters (sphere vs rod) as electrocatalysts for CO_2 reduction. The distinctly different atomic-level morphology and charge states render the Au_{25} nanosphere more active for CO_2 reduction than the Au_{25} nanorod. At −0.67 V, the nanosphere cluster exhibits a higher FE (69.3% for CO) than that of the nanorod cluster (39.7%). We have further performed DFT calculations based on their X-ray crystallographic structures and obtained mechanistic insights for the observed difference in catalytic performance. It is revealed that the negative charge state of the nanosphere as well as the energetically favorable removal of -SCH_3 from the nanosphere to expose active sites contribute to the higher catalytic features due to the stabilization of the important *COOH intermediate. This work explicitly demonstrates that the atomic-level morphology and electronic properties can greatly influence the catalytic performance; thus, the attainment of atomic structures of nanoclusters is of critical importance in order to elucidate the fundamentals of catalytic reactions. The distinct morphology dependence of nanoclusters and the obtained mechanistic insights are expected to provide some guidelines for future design of advanced catalysts for CO_2 reduction.

■ ASSOCIATED CONTENT

Supporting Information

The Supporting Information is available free of charge on the ACS Publications website at DOI: 10.1021/acscatal.8b00365.

Experimental and DFT calculation details. QQ plots of STEM on clusters, diameter histograms for the supported nanoclusters, structures of clusters with adsorbed *COOH and *CO (and H_2O formation) in DFT simulation, additional ligand removal energetics, ionization potentials and electron affinities (PDF)

■ AUTHOR INFORMATION

Corresponding Authors

*E-mail for R.J.: rongchao@andrew.cmu.edu.
*E-mail for G.M.: gmpourmp@pitt.edu.

ORCID

Stephen D. House: 0000-0003-2035-6373
Stefan Bernhard: 0000-0002-8033-1453
Giannis Mpourmpakis: 0000-0002-3063-0607
Rongchao Jin: 0000-0002-2525-8345

Notes

The authors declare no competing financial interest.

■ ACKNOWLEDGMENTS

R.J. acknowledges financial support from the Air Force Office of Scientific Research under AFOSR Award No. FA9550-15-1-9999 (FA9550-15-1-0154). G.M. acknowledges support by the National Science Foundation (NSF, CBET-CAREER program) under Grant No. 1652694 and NA support by the NSF Graduate Research Fellowship under Grant No. 1247842. G.M. and N.A. would like to acknowledge computational support from the Center for Research Computing and the Extreme Science and Engineering Discovery Environment, which is supported by the NSF (ACI-1548562). S.D.H. and J.C.Y. thank the financial support of the NSF DMREF under contract No. CHE-1534630. The electron microscopy work was performed using the facilities at the Nanoscale Fabrication and Characterization Facility, a laboratory of the Gertrude E. and John M. Petersen Institute of NanoScience and Engineering, housed at the University of Pittsburgh.

■ REFERENCES

(1) Jin, R.; Zeng, C.; Zhou, M.; Chen, Y. Atomically Precise Colloidal Metal Nanoclusters and Nanoparticles: Fundamentals and Opportunities. *Chem. Rev.* **2016**, *116*, 10346−10413.

(2) Lu, Y.; Chen, W. Sub-nanometre sized metal clusters: from synthetic challenges to the unique property discoveries. *Chem. Soc. Rev.* **2012**, *41*, 3594−3623.

(3) Ouyang, R.; Jiang, D.-e. Understanding Selective Hydrogenation of α,β-Unsaturated Ketones to Unsaturated Alcohols on the $Au_{25}(SR)_{18}$ Cluster. *ACS Catal.* **2015**, *5*, 6624−6629.

DOI: 10.1021/acscatal.8b00365
ACS Catal. 2018, 8, 4996−5001

(4) Zhao, S.; Zhang, H.; House, S. D.; Jin, R.; Yang, J. C.; Jin, R. Ultrasmall Palladium Nanoclusters as Effective Catalyst for Oxygen Reduction Reaction. *ChemElectroChem* **2016**, *3*, 1225−1229.
(5) Zeng, C.; Chen, Y.; Kirschbaum, K.; Lambright, K. J.; Jin, R. Emergence of hierarchical structural complexities in nanoparticles and their assembly. *Science* **2016**, *354*, 1580−1584.
(6) Jin, R. Quantum sized, thiolate-protected gold nanoclusters. *Nanoscale* **2010**, *2*, 343−362.
(7) Li, G.; Jin, R. Atomically Precise Gold Nanoclusters as New Model Catalysts. *Acc. Chem. Res.* **2013**, *46*, 1749−1758.
(8) Li, L.; Gao, Y.; Li, H.; Zhao, Y.; Pei, Y.; Chen, Z. F.; Zeng, X. C. CO Oxidation on TiO_2 (110) Supported Subnanometer Gold Clusters: Size and Shape Effects. *J. Am. Chem. Soc.* **2013**, *135*, 19336−19346.
(9) Kwak, K.; Choi, W.; Tang, Q.; Kim, M.; Lee, Y.; Jiang, D.-e.; Lee, D. A molecule-like $PtAu_{24}(SC_6H_{13})_{18}$ nanocluster as an electrocatalyst for hydrogen production. *Nat. Commun.* **2017**, *8*, 14723.
(10) Zhao, S.; Jin, R.; Abroshan, H.; Zeng, C.; Zhang, H.; House, S. D.; Gottlieb, E.; Kim, H. J.; Yang, J. C.; Jin, R. Gold Nanoclusters Promote Electrocatalytic Water Oxidation at the Nanocluster/$CoSe_2$ Interface. *J. Am. Chem. Soc.* **2017**, *139*, 1077−1080.
(11) Zhao, S.; Jin, R.; Song, Y.; Zhang, H.; House, S. D.; Yang, J. C.; Jin, R. Atomically Precise Gold Nanoclusters Accelerate Hydrogen Evolution over MoS_2 Nanosheets: The Dual Interfacial Effect. *Small* **2017**, *13*, 1701519.
(12) Chen, W.; Chen, S. Oxygen Electroreduction Catalyzed by Gold Nanoclusters: Strong Core Size Effects. *Angew. Chem., Int. Ed.* **2009**, *48*, 4386−4389.
(13) Wang, Q.; Wang, L.; Tang, Z.; Wang, F.; Yan, W.; Yang, H.; Zhou, W.; Li, L.; Kang, X.; Chen, S. Oxygen reduction catalyzed by gold nanoclusters supported on carbon nanosheets. *Nanoscale* **2016**, *8*, 6629−6635.
(14) Xie, S.; Tsunoyama, H.; Kurashige, W.; Negishi, Y.; Tsukuda, T. Enhancement in Aerobic Alcohol Oxidation Catalysis of Au_{25} Clusters by Single Pd Atom Doping. *ACS Catal.* **2012**, *2*, 1519−1523.
(15) Kumar, S. S.; Kwak, K.; Lee, D. Electrochemical Sensing Using Quantum-Sized Gold Nanoparticles. *Anal. Chem.* **2011**, *83*, 3244−3247.
(16) Kwak, K.; Kumar, S. S.; Lee, D. Selective determination of dopamine using quantum-sized gold nanoparticles protected with charge selective ligands. *Nanoscale* **2012**, *4*, 4240−4246.
(17) Wang, T.; Wang, D.; Padelford, J. W.; Jiang, J.; Wang, G. Near-Infrared Electrogenerated Chemiluminescence from Aqueous Soluble Lipoic Acid Au Nanoclusters. *J. Am. Chem. Soc.* **2016**, *138*, 6380−6383.
(18) Hesari, M.; Ding, Z. A Grand Avenue to Au Nanocluster Electrochemiluminescence. *Acc. Chem. Res.* **2017**, *50*, 218−230.
(19) Goswami, N.; Yao, Q.; Luo, Z.; Li, J.; Chen, T.; Xie, J. Luminescent Metal Nanoclusters with Aggregation-Induced Emission. *J. Phys. Chem. Lett.* **2016**, *7*, 962−975.
(20) Song, Y.; Fu, F.; Zhang, J.; Chai, J.; Kang, X.; Li, P.; Li, S.; Zhou, H.; Zhu, M. The Magic Au_{60} Nanocluster: A New Cluster-Assembled Material with Five Au_{13} Building Blocks. *Angew. Chem., Int. Ed.* **2015**, *54*, 8430−8434.
(21) Sakai, N.; Tatsuma, T. Photovoltaic Properties of Glutathione-Protected Gold Clusters Adsorbed on TiO_2 Electrodes. *Adv. Mater.* **2010**, *22*, 3185−3188.
(22) Abbas, M. A.; Kim, T.-Y.; Lee, S. U.; Kang, Y. S.; Bang, J. H. Exploring Interfacial Events in Gold-Nanocluster-Sensitized Solar Cells: Insights into the Effects of the Cluster Size and Electrolyte on Solar Cell Performance. *J. Am. Chem. Soc.* **2016**, *138*, 390−401.
(23) Costentin, C.; Robert, M.; Saveant, J.-M. Catalysis of the electrochemical reduction of carbon dioxide. *Chem. Soc. Rev.* **2013**, *42*, 2423−2436.
(24) Qiao, J.; Liu, Y.; Hong, F.; Zhang, J. A review of catalysts for the electroreduction of carbon dioxide to produce low-carbon fuels. *Chem. Soc. Rev.* **2014**, *43*, 631−675.
(25) Zhao, S.; Jin, R.; Jin, R. Opportunities and Challenges in CO_2 Reduction by Gold- and Silver-Based Electrocatalysts: From Bulk Metals to Nanoparticles and Atomically Precise Nanoclusters. *ACS Energy Lett.* **2018**, *3*, 452−462.
(26) (a) Zhu, W.; Michalsky, R.; Metin, Ö.; Lv, H.; Guo, S.; Wright, C. J.; Sun, X.; Peterson, A. A.; Sun, S. Monodisperse Au Nanoparticles for Selective Electrocatalytic Reduction of CO_2 to CO. *J. Am. Chem. Soc.* **2013**, *135*, 16833−16836. (b) Mistry, H.; Reske, R.; Zeng, Z.; Zhao, Z.-J.; Greeley, J.; Strasser, P.; Cuenya, B. R. Exceptional Size-Dependent Activity Enhancement in the Electroreduction of CO_2 over Au Nanoparticles. *J. Am. Chem. Soc.* **2014**, *136*, 16473−16476.
(27) Zhu, W.; Zhang, Y.-J.; Zhang, H.; Lv, H.; Li, Q.; Michalsky, R.; Peterson, A. A.; Sun, S. Active and Selective Conversion of CO_2 to CO on Ultrathin Au Nanowires. *J. Am. Chem. Soc.* **2014**, *136*, 16132−16135.
(28) Lee, H.-E.; Yang, K. D.; Yoon, S. M.; Ahn, H.-Y.; Lee, Y. Y.; Chang, H.; Jeong, D. H.; Lee, Y.-S.; Kim, M. Y.; Nam, K. T. Concave Rhombic Dodecahedral Au Nanocatalyst with Multiple High-Index Facets for CO_2 Reduction. *ACS Nano* **2015**, *9*, 8384−8393.
(29) Cao, Z.; Kim, D.; Hong, D.; Yu, Y.; Xu, J.; Lin, S.; Wen, X.; Nichols, E. M.; Jeong, K.; Reimer, J. A.; Yang, P.; Chang, C. J. A Molecular Surface Functionalization Approach to Tuning Nanoparticle Electrocatalysts for Carbon Dioxide Reduction. *J. Am. Chem. Soc.* **2016**, *138*, 8120−8125.
(30) Kim, K.-S.; Kim, W. J.; Lim, H.-K.; Lee, E. K.; Kim, H. Tuned Chemical Bonding Ability of Au at Grain Boundaries for Enhanced Electrochemical CO_2 Reduction. *ACS Catal.* **2016**, *6*, 4443−4448.
(31) Kim, J.-H.; Woo, H.; Choi, J.; Jung, H.-W.; Kim, Y.-T. CO_2 Electroreduction on Au/TiC: Enhanced Activity Due to Metal−Support Interaction. *ACS Catal.* **2017**, *7*, 2101−2106.
(32) Back, S.; Yeom, M. S.; Jung, Y. Active Sites of Au and Ag Nanoparticle Catalysts for CO_2 Electroreduction to CO. *ACS Catal.* **2015**, *5*, 5089−5096.
(33) Kauffman, D. R.; Alfonso, D.; Matranga, C.; Qian, H.; Jin, R. Experimental and Computational Investigation of Au_{25} Clusters and CO_2: A Unique Interaction and Enhanced Electrocatalytic Activity. *J. Am. Chem. Soc.* **2012**, *134*, 10237−10243.
(34) Kauffman, D. R.; Alfonso, D.; Matranga, C.; Ohodnicki, P.; Deng, X.; Siva, R. C.; Zeng, C.; Jin, R. Probing active site chemistry with differently charged Au_{25}^q nanoclusters (q = −1, 0, + 1). *Chem. Sci.* **2014**, *5*, 3151−3157.
(35) Kauffman, D. R.; Thakkar, J.; Siva, R.; Matranga, C.; Ohodnicki, P. R.; Zeng, C.; Jin, R. Efficient Electrochemical CO_2 Conversion Powered by Renewable Energy. *ACS Appl. Mater. Interfaces* **2015**, *7*, 15626−15632.
(36) Alfonso, D. R.; Kauffman, D.; Matranga, C. Active sites of ligand-protected Au_{25} nanoparticle catalysts for CO_2 electroreduction to CO. *J. Chem. Phys.* **2016**, *144*, 184705.
(37) Wu, Z.; Suhan, J.; Jin, R. One-pot synthesis of atomically monodisperse, thiol-functionalized Au_{25} nanoclusters. *J. Mater. Chem.* **2009**, *19*, 622−626.
(38) Qian, H.; Zhu, M.; Lanni, E.; Zhu, Y.; Bier, M. E.; Jin, R. Conversion of Polydisperse Au Nanoparticles into Monodisperse Au_{25} Nanorods and Nanospheres. *J. Phys. Chem. C* **2009**, *113*, 17599−17603.
(39) Zhu, M.; Aikens, C. M.; Hollander, F. J.; Schatz, G. C.; Jin, R. Correlating the Crystal Structure of A Thiol-Protected Au_{25} Cluster and Optical Properties. *J. Am. Chem. Soc.* **2008**, *130*, 5883−5885.
(40) Shichibu, Y.; Negishi, Y.; Watanabe, T.; Chaki, N. K.; Kawaguchi, H.; Tsukuda, T. Biicosahedral Gold Clusters $[Au_{25}(PPh_3)_{10}(SC_nH_{2n+1})_5Cl_2]^{2+}$ (*n* = 2−18): A Stepping Stone to Cluster-Assembled Materials. *J. Phys. Chem. C* **2007**, *111*, 7845−7847.
(41) Perdew, J. P.; Burke, K.; Ernzerhof, M. Generalized Gradient Approximation Made Simple. *Phys. Rev. Lett.* **1996**, *77*, 3865−3868.
(42) VandeVondele, J.; Hutter, J. Gaussian basis sets for accurate calculations on molecular systems in gas and condensed phases. *J. Chem. Phys.* **2007**, *127*, 114105.
(43) Goedecker, S.; Teter, M.; Hutter, J. Separable dual-space Gaussian pseudopotentials. *Phys. Rev. B: Condens. Matter Mater. Phys.* **1996**, *54*, 1703−1710.

DOI: 10.1021/acscatal.8b00365
ACS Catal. 2018, 8, 4996−5001

(44) VandeVondele, J.; Krack, M.; Mohamed, F.; Parrinello, M.; Chassaing, T.; Hutter, J. Quickstep: Fast and accurate density functional calculations using a mixed Gaussian and plane waves approach. *Comput. Phys. Commun.* **2005**, *167*, 103−128.
(45) Li, G.; Abroshan, H.; Chen, Y. X.; Jin, R. C.; Kim, H. J. Experimental and Mechanistic Understanding of Aldehyde Hydrogenation Using Au_{25} Nanoclusters with Lewis Acids: Unique Sites for Catalytic Reactions. *J. Am. Chem. Soc.* **2015**, *137*, 14295−14304.
(46) Li, G.; Abroshan, H.; Liu, C.; Zhuo, S.; Li, Z. M.; Xie, Y.; Kim, H. J.; Rosi, N. L.; Jin, R. Tailoring the Electronic and Catalytic Properties of Au_{25} Nanoclusters via Ligand Engineering. *ACS Nano* **2016**, *10*, 7998−8005.
(47) Henkelman, G.; Arnaldsson, A.; Jonsson, H. A fast and robust algorithm for Bader decomposition of charge density. *Comput. Mater. Sci.* **2006**, *36*, 354−360.
(48) Peterson, A. A.; Abild-Pedersen, F.; Studt, F.; Rossmeisl, J.; Norskov, J. K. How copper catalyzes the electroreduction of carbon dioxide into hydrocarbon fuels. *Energy Environ. Sci.* **2010**, *3*, 1311−1315.
(49) House, S. D.; Chen, Y.; Jin, R.; Yang, J. C. High-throughput, semi-automated quantitative STEM mass measurement of supported metal nanoparticles using a conventional TEM/STEM. *Ultramicroscopy* **2017**, *182*, 145−155.

DOI: 10.1021/acscatal.8b00365
ACS Catal. 2018, 8, 4996−5001